Automatic Detection of Aquatic Weeds: A Case Study in the Guadiana River, Spain

Elena C. Rodríguez-Garlito, *Student Member, IEEE*, Abel Paz-Gallardo, and Antonio Plaza, *Fellow, IEEE*

***Abstract*—The spread of aquatic invasive plants is a major concern in several zones of the world's geography. These plants, which are not part of the natural ecosystem, cause a negative impact to the environment, as well as to economy and society. In Spain, large areas of Guadiana (the second-longest river in Spain) have been invaded by such plants. Among the strategies to address this problem, monitoring and detection play an important role to control the spatiotemporal distribution of the invasive plants. The main objective of this work is to develop a methodology able to automatically detect the geolocation of aquatic invasive plants using remote sensing and machine learning techniques. To this end, several classification algorithms have been applied to freely available multispectral satellite imagery, collected by ESA's Sentinel-2 satellite. A quantitative and comparative assessment is conducted using different machine and deep learning algorithms from classical methods, such as unsupervised K-means to supervised random forests and convolutional neural networks. This study also proposes a methodology for validating the obtained classification results, generating synthetic ground truth images based on available high spatial resolution imagery. The obtained results demonstrate the suitability of some of the considered algorithms for automatic detection of aquatic weeds in satellite images with medium spatial resolution.**

***Index Terms*—Aquatic weeds, deep learning (DL), detection, invasive plants, machine learning (ML), remote sensing (RS), Sentinel-2.**

I. Introduction

REMOTE sensing (RS) and geographical information systems (GISs) are two disciplines on the rise in recent decades. Together, they provide an ideal analysis framework in many disciplines [1]. Based on RS technology, multispectral (MS) or hyperspectral (HS) sensors installed on airborne (airplanes/drones) or spaceborne (satellites) platforms measure the energy that an object in the Earth's surface reflects and absorbs. In this way, MS or HS images record measurements in discrete and discontinuous portions of the spectral range, with tens (MS) or hundreds (HS) of nearly contiguous spectral bands. As a result, RS data contain a vast amount of information in the spatial and spectral domains and can be represented as data cubes, as they comprise data in three dimensions [2]. In other words, each pixel is composed of tens or hundreds of measurements in different wavelengths.

On the other hand, GIS technology facilitates the understanding of the information in the pixels that make up the data cube by taking advantage of the information available in the spatial domain. In this way, maps can be created displaying the spectral observations in a georeferenced way. This also allows for the arrangement of different layers of georeferenced information for better assessment of the data using GIS techniques in computer applications.

The exploitation of RS together with GIS exhibits the potential to improve the understanding of the land surface, thanks to the detailed information that RS images provide, consequently allowing for a precise analysis and GIS-based interpretation that is applicable to several fields, such as urban planning [3], biodiversity [4], disaster management [5], precision agriculture [5], land cover mapping [6], monitoring of oil spills and other events [7], among many others. In particular, classification allows distinguishing water bodies from other impervious surfaces (e.g., urban environments), including soil and vegetation. This allows us to address problems related to (for instance) the excessive growth of vegetation in water (the most important resource on the planet).

The inefficient management of domestic, agricultural, or industrial waste contributes to the excess of nutrients in aquatic ecosystems (e.g., phosphorus and nitrogen), which pollute the water through a process called eutrophication [8]. Important ecological impacts, such as the loss of water quality, stem from the enrichment of nutrients in the water. This enrichment also causes an excessive growth of certain plant species known as aquatic weeds [9]. An excessive presence of such weeds could lead to the fact that a large amount of oxygen dissolved in the water is consumed during their growth and putrefaction, introducing a large amount of organic matter in the water [10]. Most notably, floating aquatic weeds tend to create a mantle on the surface of the water that absorbs light, reducing the amount of illumination in benthic habitats and, therefore, reducing biodiversity [11].

Manuscript received 18 July 2022; revised 5 September 2022; accepted 26 September 2022. Date of publication 28 September 2022; date of current version 12 October 2022. This work was supported in part by European Social Fund (Resolución de 10 de mayo de 2017, de la Secretaría General de Ciencia, Tecnología e Innovación, por la que se resuelve la convocatoria de ayudas para la financiación de contratos predoctorales para formación de Doctores en los centros públicos de I+D pertenecientes al Sistema Extremeño de Ciencia, Tecnología e Innovación en el ejercicio 2017 expediente PD16001), in part by the Consejería de Economía, Ciencia y Agenda Digital of the Junta de Extremadura and the European Regional Development Fund (ERDF) of the European Union under Grant GR21040, in part by Spanish Ministerio de Ciencia e Innovacion under Grant PID2019-110315RB-I00 (APRISA), and in part by European Union's Horizon 2020 Research and Innovation Program under Grant 734541 (EOXPOSURE). *(Corresponding author: Antonio Plaza.)*

The authors are with the Hyperspectral Computing Laboratory, Department of Technology of Computers and Communications, Escuela Politécnica, University of Extremadura, 10003 Cáceres, Spain (e-mail: elenacristinarg@unex.es; apazgal@unex.es; aplaza@unex.es).

Digital Object Identifier 10.1109/JSTARS.2022.3210373

Occasionally, in specific geographical areas on the water's surface, there is vegetation that is not part of that particular ecosystem. Such kind of vegetation is also referred to as alien species. These are invasive species introduced intentionally or accidentally, e.g., due to globalization (trade, transport of goods, etc.). Due to their invasive nature, these species also pose a significant threat to the species of the native ecosystem [12]. Therefore, the removal of these so-called invasive plants is much needed to reduce the impact introduced in the environment and water quality, and also to reduce the negative economic impact [13]. As a specific case study, the Guadiana river basin in Extremadura (a region in the southwest of Spain) contains invasive species, such as water hyacinth (*Eichhornia crassipes*), since the beginning of the 2000s. It is possible to perform mechanical elimination of these species by chemical or biological means [14], [15], as well as to adopt other methods to control their spread [16].

In order to monitor and control invasive aquatic plants, mapping their distribution is a critical step. RS plays an important role in this task, since satellite images provide rich spatial and temporal information. In recent decades, we have seen a tremendous growth of RS studies in which image analysis and different sensor specifications have been exploited to map and detect aquatic invasive plants [17], [18], [19], [20], [21]. However, in the literature, there are few studies aimed at monitoring and controlling of aquatic invasive plants using machine learning (ML) techniques [22], [23], [24].

Artificial intelligence (AI) approaches provide a wide variety of regression and classification algorithms for the interpretation of RS images. Besides, depending on the availability of labeled samples to train the models, they can be categorized into unsupervised, supervised, or semisupervised methods (a hybrid of the first-two). Popular examples of unsupervised methods are clustering algorithms. These algorithms find natural groups with similar spectral behavior, such as the well-known K-means. Due to its simplicity, this method has been widely used to group samples of data in clusters [25]. On the other hand, supervised algorithms, such as random forests (RFs) [26], support vector machines [27], K-nearest neighbor [28], or multilayer perceptron (MLP), require training samples. MLP is in fact an artificial neural network (ANN), which mimics the behavior of neurons in the human brain. ANN-based algorithms have significantly developed in recent years, thanks to the advent of computer hardware, such as graphics processing units, and have evolved into a subfield of ML called deep learning (DL). Numerous studies have considered DL algorithms [29]. Among them, convolutional neural networks (CNNs) have become extremely popular due to their outstanding performance in many classification tasks (e.g., to recognize objects [30], scenes [31], pixel classification of a scene [32], or subpixel detection [33]).

The main goal of this work is to develop an ML/DL methodology to automatically detect the spatial–temporal distribution of aquatic invasive plants in the Guadiana river. To the best of our knowledge, there are no previous studies about the detection of aquatic weeds in this river combining GIS, RS, and AI techniques [34]. Specifically, we could not find any works using DL to address this problem. The main innovative contributions of our work can be summarized as follows.

1) We establish a full processing chain, including preprocessing, processing, and evaluation, of Sentinel-2 images, using RS and GIS tools (with treatment of NoData values), to automatically detect invasive aquatic weeds in the Guadiana river.
2) We have implemented a novel strategy to validate the performance of ML/DL algorithms in the considered application. To be specific, we generate synthetic ground truth (GT) data from a high-resolution MS image. For this purpose, we use data acquired by the (Spanish) National Plan of Aerial Orthophotography (PNOA) that provides open-access datasets that have been preclassified using a window-based processing strategy [35].
3) We carry out a detailed comparison between ML and DL algorithms in the context of aquatic weeds detection. In order to show that invasive aquatic plants can be monitored using ML/DL techniques, two areas in the Guadiana river, Spain, have been carefully selected and studied. K-means clustering and the RF algorithm have been applied to them, and a CNN architecture has also been configured for this study. We use Sentinel-2 medium-resolution MS images to conduct the study, as they can be collected with a frequent revisit time (five days) and are freely available to the scientific community. We also report results on the full Sentinel-2 flightlines for reference.

The rest of this article is organized as follows. Section II describes some challenges related to the detection of aquatic weeds in the Guadiana river. Section III outlines some available open-access RS datasets to detect aquatic weeds in the Guadiana river. Section IV describes the adopted ML/DL techniques. Section V explains the materials and methods used in our work. Section VI discusses the obtained experimental results. Finally, Section VII concludes this article.

II. Aquatic Weeds in the Guadiana River: Background and Challenges

The challenge of preventing and controlling the existence and spread of invasive aquatic weeds extends over a large part of the world geography. As an illustration, the water hyacinth (*Eichhornia crassipes*) is one of the most invasive species on the Earth. Its geographical distribution reaches almost every continent [36]. In Africa, it is present in many places, such as the Lake Victoria or Niger river. In Asia, it can be found at the Al Kabir river. In Australia, it covers the Burdeki Riverand. And, in North and South America, it is present in the Rio Grande and several lagoons outside the Amazon, among others. In Europe, these aquatic weeds are also living in France, Italy, Portugal, Germany, and Spain, where the second-largest river (Guadiana) is largely affected.

The Guadiana river's basin is located at the Iberian Peninsula and covers an area of about 67 129.38 km^2. The river flows in a course of about 829 km from east to west, extending for the most part in the southwest of Spain. The Spanish basin crosses the regions of Andalucía, Castilla La Mancha, and Extremadura,

Fig. 1. *Nymphaea mexicana* in the Guadiana river, photographed by Tomás Rodríguez.

distributed in an area of 55 508.28 km^2 [37]. In this work, we focus on two areas located in Extremadura, where the basin of the Guadiana river occupies an area of 23 443.73 km^2. Moreover, Extremadura has about 1500 km of inland coastline, the largest in Western Europe.

In addition to *Eichhornia crassipes*, other invasive aquatic plant species have spread in the Guadiana river, such as *Nymphaea mexicana* (see Fig. 1) and *Azolla filiculoides*. They all have American origin. Moreover, as shown in Fig. 1, their tapestry-like distribution on the surface of the water prevents the passage of light and affects native vegetation as well as aquatic invertebrates [38], [39], [40]. The negative ecological and socioeconomic impacts caused by these invasive plants have motivated different control mechanisms, as well as eradication attempts by public institutions. In this sense, several extraction and surveillance actions have been carried out, requiring large economic investments. Some of these actions have been framed within international projects [41], [42], including LIFE + INVASEP "Combat invasive species in the Tajo and Guadiana drainage basins in the Iberian Peninsula," Interreg Spain–Portugal LIFE10/NAT/ES 000582, and ACECA Project—cofinanced by the European Regional Development Fund (i.e., FEDER)—with budgets of 2 895 267 and 5 560 221.66 euros in 2012–2016 and 2014–2020 periods, respectively.

The current strategies carried out for the eradication of invasive aquatic plants have not achieved their total elimination. In this regard, new financial investments for control strategies are planned for the 2021–2027 period for *Eichhornia crassipes* and *Nymphaea mexicana* [43], respectively. For this reason, monitoring and mapping aquatic weeds are necessary. RS and GIS techniques for image acquisition and processing are powerful tools for this purpose.

III. Open-Access RS Datasets

There is a wide variety of currently operational RS instruments able to capture spectral radiance or reflectance of the Earth's surface, with different numbers of spectral channels covering a diversity of spectral ranges. On the one hand, HS sensors collect data in hundreds of nearly contiguous spectral bands. On the other hand, MS images usually have a lower discrete number of bands. RS sensors are flown on airborne or spaceborne instruments, taking part in different space missions or national plans, which provide coverage throughout international and national territories, in several formats and resolution in the spatial, spectral, and temporal domains. RS imagery are often available for free or under request. In our research, medium-resolution images (acquired with frequent revisit times) have been targeted to monitor the spread of aquatic invasive plants. Whenever available, open-access databases have been chosen. In that sense, the MS dataset provided by PNOA and datasets collected by Sentinel-2 have been selected.

Several research efforts have considered digital aerial orthophotographs collected by PNOA for photointerpretation tasks, due to their high spatial resolution [44], [45], [46]. Some projects managed by the Ministry of Development (Spain) follow the INSPIRE Directive [47], which establishes a spatial data infrastructure for geographic data in Europe to provide geometric and temporal coherence of cartographic and geographic databases. In this way, aerial photography constitutes a basis for the realization of information on urban planning, land occupation, hydrography, forest management, and cartography for territories belonging to the European Community. Within the PNOA framework, it is possible to perform photogrammetric flights using planes equipped with a high-resolution digital camera, four MS sensors, and a panchromatic sensor, collecting high spatial resolution images (25 or 50 cm) of the entire Spanish

TABLE I
SENTINEL-2 BANDS

Band name	B01	B02	B03	B04	B05	B06	B07	B08	B8A	B09	B10	B11	B12
Resolution (m)	60	10	10	10	20	20	20	10	20	60	60	20	20
Bandwidth (nm)	442.7	492.4	559.8	664.6	704.1	740.5	782.8	832.8	864.7	945.1	1373.5	1613.7	2202.4
Application	Coastal aerosol	Blue	Green	Red	Vegetation red edge	Vegetation red edge	Vegetation red edge	NIR	Narrow NIR	Water vapour	Cirrus	SWIR	SWIR

territory within a period of 2 or 3 years (depending on the area) [48]. Among the products offered, PNOA provides free MS images with high spatial resolution and three RGB spectral bands in the European Terrestrial Reference System (ETRS89) geodetic system. Furthermore, upon request, digital frames of PNOA flights can be purchased. These images comprise four bands, three for the visible (RGB) part of the spectrum and one for near-infrared (NIR), all georeferenced in the ETRS89 geodetic Cartesian reference framework, with high spatial resolution images (0.22 or 0.45 m).

Last but not least, the European Space Agency (ESA) developed (as part of the Copernicus programme) a family of Earth observations missions called Sentinels. In this work, given their success for land cover classification [49], [50], an MS medium-resolution optical imagery provided by Sentinel-2 mission (focused on land monitoring [51]) is considered. Sentinel-2 provides coverage over all land areas, except Antarctica, via two identical satellites, which are composed by an MS instrument (whose technical characteristics allow a revisit time of five days). Sentinel-2 offers two types of products: 1) Level-1 C (S2L1C); and 2) Level-2 A (S2L2A). Both of them are available for free, and they are composed of 100×100 km^2 tiles, which are orthoimages in UTM/WGS84 projection. S2L1C is a top-of-atmosphere reflectance product and S2L2A a bottom-of-atmosphere reflectance product. S2L2A is the result of applying atmospheric correction techniques to S2L1C images (thanks to a processing algorithm called Sen2Cor, developed by ESA). As a result, the reflection and scattering of light by the atmosphere before reaching the ground is corrected. Each S2L1C image is composed of 13 spectral bands, containing reflectance values from the visible and NIR to the shortwave infrared, with spatial resolutions of 10-, 20-, and 60-m per pixel (depending on the wavelength). In this way, the four visible spectral bands have spatial resolution of 10-m per pixel, the six NIR bands have 20-m spatial resolution, and the three shortwave infrared bands have 60-m spatial resolution. In case of S2L2A, the B10 band (used for cirrus cloud detection) is excluded, because it does not contain any information at the bottom of the atmosphere (see Table I [52]).

IV. MACHINE/DEEP LEARNING TECHNIQUES

To the best of our knowledge, AI methods have not been fully explored as of yet to automatically map the spatiotemporal distribution of aquatic invasive plants. In this section, we describe some ML/DL techniques that we have used to perform automatic invasive plants detection.

Let an MS image be defined by $X \in \mathbb{R}^{H \times W \times B}$, where H and W denote the height and width of the data cube, respectively, and B is the number of spectral bands. The goal is to find a mapping function $\mathcal{M}_\theta : X \to Y$ that assigns each pixel x_i to a corresponding label y_i (including aquatic weed), producing a classification map $Y \in \mathbb{R}^{H \times W}$. In this sense, ML/DL algorithms build a model based on learning to make predictions. In supervised approaches, training samples are collected and labels for some pixels are available (e.g., by means of a human-based annotation process). On the contrary, unsupervised approaches group similar pixels together by discovering patterns of similarity. Last but not least, semisupervised methods combine labeled and unlabeled data during the training process.

Recent advances in ML/DL algorithms, high-performance computing, and Big Data accessibility have led to the adoption of ANNs for classification tasks [53]. DL, which can be considered as a subfield of ML [54], exploits many ANN layers that are stacks of functions able to extract features at different levels [55]. Their structure exhibits great advantages over traditional ML algorithms. Specifically, DL models can be adapted to supervised and unsupervised classification tasks; their learning procedure allows to extract linear and nonlinear features, and they exhibit great flexibility in their architectures, thanks to their diversity in terms of both the types of layer that can be arranged and their number (depth) [56].

In the following, general aspects of the ML/DL algorithms adopted in our work are given. Specifically, we use an unsupervised method widely known for its simplicity (i.e., K-means clustering), a supervised (i.e., RF) based on decision trees, and a supervised DL method (i.e., CNN).

1) K-means: K-means is a popular unsupervised method among clustering techniques where data are grouped in clusters such that samples in the same group (or cluster) are more similar to each other than those in other groups. The goal of this algorithm is to choose centroids within a cluster sum-of-squares criterion given by

$$\sum_{i=0}^{n} \left(\| x_i - \mu_j \|^2 \right) \quad (1)$$

where n is the number of groups of equal variance in which samples are separated and x_i are the samples (divided into k disjoint clusters C described by the mean μ_j). The operation of this algorithm can be described in several steps.

a) In the first step, parameter k (corresponding to the number of clusters to be identified in the data) is set. Then, the centroids of the clusters are chosen and each sample is assigned to its nearest centroid.

b) In the second step, new centroids are created by taking the mean value of all the samples assigned to each previous centroid. The difference between the new centroids and the old ones is computed, and this process is repeated until there are no more changes in the location of the centroids.

2) Random Forest: RF is an ensemble learning approach first introduced in [57]. In particular, this method classifies pixels by creating a multitude of randomized decision trees (supervised and nonparametric classifiers) where the final prediction is an average of the probabilistic ones of each decision tree. In other words, it performs a bagging strategy by building the trees from top to bottom based on the "divide and conquer" concept [58], achieving error compensations. First, in order to carry out the (supervised) classification, a training set is defined. RF operates by means of a bagging procedure in which training samples are randomly selected from the original training set. As a result, some samples may not be used and others may be chosen more than once. Next, each decision tree is built with different training sets by using a boostrapped dataset. This technique improves the generalization of the learning process by avoiding the tendency to overfitting of decision trees. It is advantageous for reducing model variance without increasing bias. Other methods based on "boosting" are more sensitive to overtraining and noise [59].

3) Convolutional Neural Networks: CNNs are a kind of nonlinear models categorized within a supervised deep network (discriminative deep networks). Their structure is inspired by the behavior of neurons in visual neuroscience. CNNs comprise a set of blocks with units (or neurons) capable to transform the input data volume to an output volume of units (or neurons). The output volume of neurons of the previous blocks will be the input block to the following block [32]. In general terms, as any feedforward neural network, the architecture of the CNN consists of an input layer, hidden layers, and output layer. The hidden layers are divided in two parts: a) the first one is the feature extractor; and b) the second part is often an MLP, which assigns the final class labels. In other words, this design consists of multiple layers where the outer layers of a CNN extract basic features, whereas more complex learning is hierarchically produced in the inner layers. With regards to the MLP, the neurons of a layer are not fully connected to all neurons of the previous one, because they are connected to a small region of previous input volume. This particularity allows the blocks of neurons in a CNN to work as kernels, operating over a small region of the previous layer. The withdrawal of fully connected layers can be beneficial in terms of reducing complexity and enhancing the exploitation of spatial information in the data. CNNs have been successfully applied to perform RS image classification. Their multilayer structure can exploit the advantages of natural signal sharing weights, with pooling layers and local connections. The way input data are presented to the network (in the form of multiple arrays), makes it suitable to process both MS and HS images [60]. The main types of hierarchical structures are convolutional layers with nonlinear operation and pooling layers in the first stages and fully connected layers in the last stages [56]. The CNN applies weights and biases to the input data in each hidden layer. CNNs use an activation function and perform convolutions. Among the different types of CNN models for RS data classification (spectral CNN, spatial CNN, and spectral–spatial CNN) [61], we focus on spectral CNNs [62] where the procedure repeated in the convolutional layers l can be described as

$$l : X_k^l = \sigma(K_1^{l-1} * X^{l-1} + b_k^{l-1}) \tag{2}$$

where the feature map created at each layer l is X_k, K is a set of kernels $K = \{K_1, K_2, K_3, \ldots, W_k\}$, the b applied biases are $\gamma = \{b_1, b_2, b_3, \ldots, b_k\}$, the input RS dataset is convolved using the $*$ operation, and the nonlinear transform function is denoted by $\sigma(.)$ [29]

V. Materials and Methods

A. Study Area

Our study has been conducted at the Guadiana river in Extremadura, Spain. Two portions of a section affected by aquatic weeds in the river have been analyzed. The first region of interest (ROI) corresponds to a section affected by *Nymphaea mexicana* that crosses the city of Badajoz (denoted hereinafter as BA_zone) with an area of 192 ha approximately, which extends between 7° 01′–6° 58′ W latitude and 38° 51′–38° 53′ N longitude. The second study area (about 45 ha) is affected by *Eichhornia crassipes* in the city of Mérida (denoted hereinafter as ME_zone) in which an invasive plant control barrier has been installed in the river for mechanical removal. This area extends between 6° 19′–6° 18′ W latitude and 38° 50′–38° 51′N longitude, respectively (see Fig. 2).

B. MS Datasets

In our experiments, several datasets collected by different MS sensors (PNOA and Sentinel-2) have been considered. First, to facilitate the training and validation for aquatic weeds detection, the PNOA dataset has been obtained over BA_zone and ME_zone. The orthophotographs have been obtained for free from National Geographic Institute's Download Center (IGN) [63]. By analyzing the metadata of each image, we can see that the date in which they were collected was July 10, 2019. These PNOA datasets include three RGB bands and their dimensions are 18 630 × 9747 and 7443 × 6321 pixels (width × height) for the BA_zone and ME_zone, respectively. As will be explained later, both images acquired by the PNOA are rectangular and include both ROIs for Badajoz and Mérida (i.e., ROI_BA and ROI_ME), corresponding to the river areas being analyzed, as well as some NoData values (pixels where there is no information). There are 27 448 554 and 6 432 601 pixels with information in ROI_BA and ROI_ME, respectively, with a spatial resolution of 0.25-m per pixel. These datasets were downloaded in Unit 8 (unsigned integer 8 bits) format, where each pixel values range from 0 to 255.

Our study aims to detect aquatic weeds by using free high spatial resolution satellite images with a frequent revisit time over the ROI, allowing for the monitoring and control of the weeds. For this purpose, datasets S2L2A (acquired by an MS sensor onboard Sentinel-2) have been downloaded from a satellite imagery provider called SentinelHub [64]. These datasets are

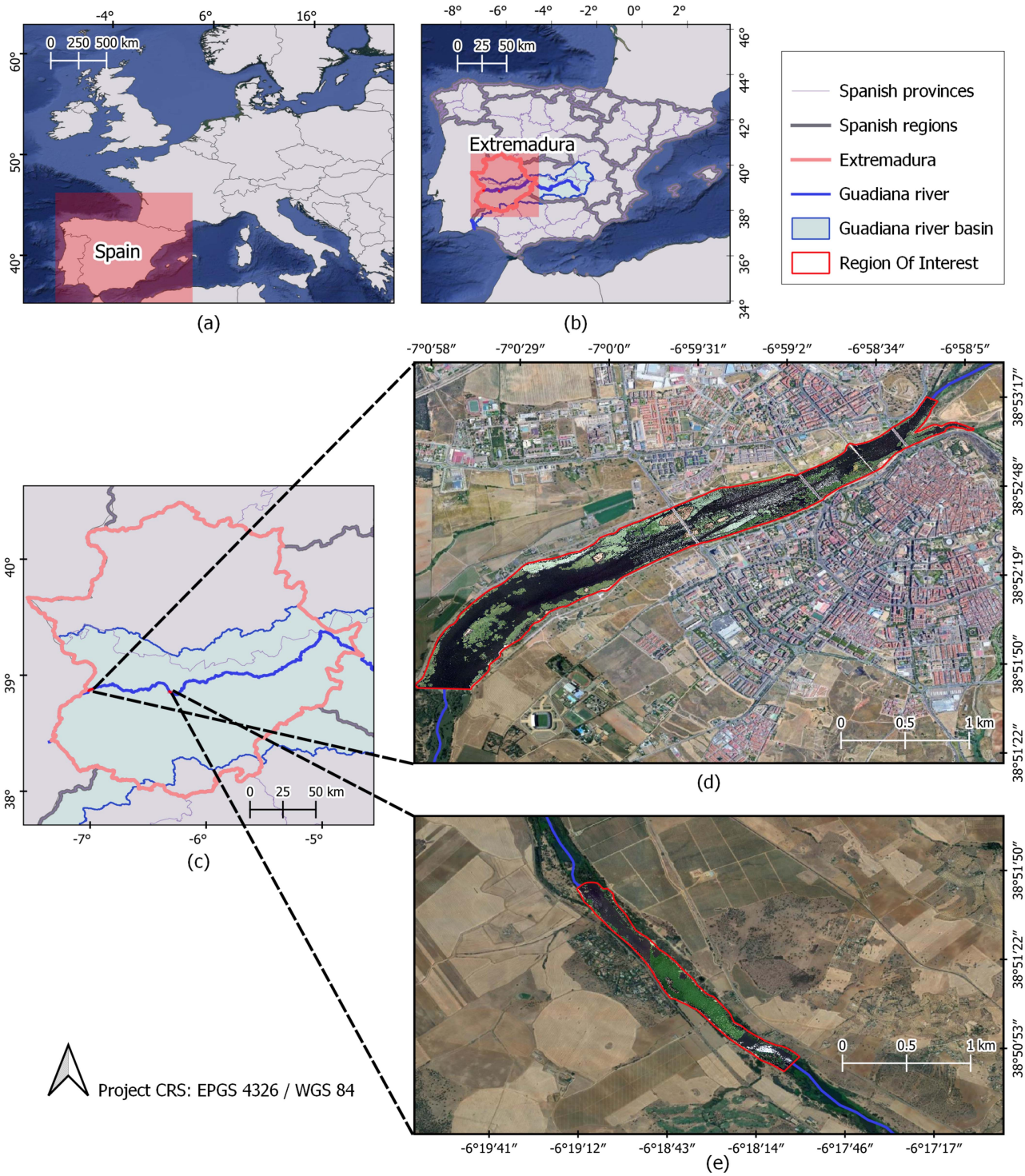

Fig. 2. (a) Geographical location of Spain. (b) Geographical location of the region of Extremadura, the Guadiana river, and the Guadiana river basin. (c) Zoom of the Extremadura region, depicting the Guadiana river and its basin. (d) Zoom of an area affected by aquatic weeds in Badajoz city (BA_zone). (e) Zoom of an area affected by aquatic weeds in Mérida city (ME_zone).

atmospherically corrected so they are not foggy in appearance (as it is the case of S2L1C datasets). Since Sentinel-2 has a revisit time of five days, the closest date to the PNOA datasets has been chosen. For BA_zone and ME_zone, images from July 11, 2019, have been downloaded. These MS datasets contain 12 bands ranging from 442.7 to 2202.4 nm, with spatial resolution of 10-, 20-, or 60-m per pixel, depending on the wavelength. Table III gives the corresponding bands. After applying a clipping mask with ROI_BA, the S2L2A dataset for BA_zone has dimensions of 451 $\times$ 236 pixels, being 16 240 pixels with information (the rest are NoData values). In the case of ME_zone, the S2L2A dataset has dimensions of 189 $\times$ 173, with 4471 pixels with

information. Both MS images have been downloaded in 8 bit format (unsigned integer 8 bits), where the pixel values range from 0 to 255.

C. Hardware/Software Environment

The hardware environment used in the experiments is composed by an Intel(R) Core(TM) i7-8700 processor, 32 GB random access memory (RAM) memory, and 1 TB SSD. The window partitioning strategy and the ML/DL frameworks have been implemented in Python 3.8 programming language, selected because of its open-source nature, its versatility, and flexible integration with other components, in addition to the existence of numerous libraries. In addition, a very popular DL framework has been used, i.e., TensorFlow, which is an end-to-end open-source platform which is very easy to use through the high-level library Keras (a DL application programming interface). Regarding image preprocessing operations, most of them have been carried out using QGIS software [65], as well as tools developed in QGIS. In general terms, GIS techniques have been used for the following.

1) Visualization of images (PNOA, Sentinel-2, and classified images).
2) Treatment of NoData values, i.e., to query pixel values, and to analyze histograms, spectral signatures, etc.
3) *Training sample collection process:* This has been accomplished by means of vectors (polygons) drawing over the Sentinel-2 image, having as a reference layer, the PNOA high-resolution image. The samples were extracted from the Sentinel-2 image.
4) *Data preprocessing and postprocessing:* All previous tools were used directly on QGIS, but also implemented in Python to automate processes.
5) Maps layout design (for better understanding when displaying results).
6) The synthetic GT generation (described in Section V-G2) was performed using a Python script to automate all GIS processes needed (crop geolocation, centroids generation, vectorial data calculations, etc.).

D. Classification Methods

In order to verify that aquatic weeds can be automatically detected by ML/DL algorithms, the following methods have been adopted.

1) K-Means: The number of classification groups (the same number of centroids generated) has been set empirically using different values (between 3 and 6) in order to classify the two scenarios according to their most representative classes (four and five classes for ROI_ME and ROI_BA, respectively).

2) Random Forest: The number of estimators has been set to 100 after checking that the obtained results did not improve much by increasing the number of decision trees. They have been tested with an increasing value of tree depth, since the algorithm takes longer after a certain depth, but the accuracy remains the same.

3) Convolutional Neural Network: The CNN is applied in such a way that the spectral signature of each pixel is considered as the input vector. Therefore, the CNN receives as many input vectors as the number of pixels in the MS image. It is assumed each pixel is labeled as one class. The structure of our CNN classifier consists of several layers, i.e., convolutional, reshaping, fully connected, normalization, and activation, as shown in Fig. 3. In this study, the CNN does not use spatial information (only spectral information), due to the fact that we are using a 1-D convolutional network (CNN1D). This makes a fair comparison with the other ML algorithms used (i.e., K-means and RF).

TABLE II
NUMBER OF TRAINING SAMPLES (PIXELS) USED FOR TRAINING THE RF AND CNN CLASSIFIERS IN THE BADAJOZ AND MÉRIDA CASES

Number of training samples (pixels)	Badajoz case	Mérida case
Water	176	101
Aquatic weeds	195	162
Soil	8	10
Other vegetation	22	177
Other	18	–
Total number and percentage of training samples used	419 (2.58%)	450 (10.06%)
Total number of labeled pixels inside each ROI	16 240	4471

The numbers in the parentheses are the percentage of the total number of labeled samples used for training in each case (rest of the labeled samples were used for testing)

E. Training and Validation

In order to apply supervised classification algorithms, we choose a set of training samples from Sentinel-2 images for each of the scenarios analyzed in this article. Since the PNOA images have higher spatial resolution and have been taken at the same date as the Sentinel-2 images, two training datasets have been defined by photointerpretation over PNOA images. The first training dataset has been selected according to the predominant classes in the ROI_BA scenario, so that representative samples have been collected from each of them. Specifically, five classes (i.e., water, aquatic weeds, soil, other vegetation, and other as bridges) were defined in ROI_BA. Similarly, samples from four representative classes (i.e., water, aquatic weeds, soil, and other vegetation) have been selected in ROI_ME. First, samples were taken with pixels containing only a single class. As we were mainly interested in locating invasive plants in this study, for greater accuracy of results, we proceeded to take training samples of mixed pixels containing invasive plants among other classes. The segmentation process of these training samples was carried out using GIS tools in QGIS software. Table II gives the total number of pixels used for training the RF and CNN classifiers in both scenarios. The numbers in the parentheses are the percentage of available labeled samples used for training, while the rest of the labeled samples were used for testing. As it can be seen in Table II, the RF and CNN classifiers are trained with a very limited number of the available labeled pixels (2.58% of the labeled samples for the Badajoz case and 10.06% of the labeled samples for the Mérida case).

The training sets (one for BA_zone and one for ME_zone) include samples of invasive plants and other classes that are not invasive plants (with other kinds of vegetation among

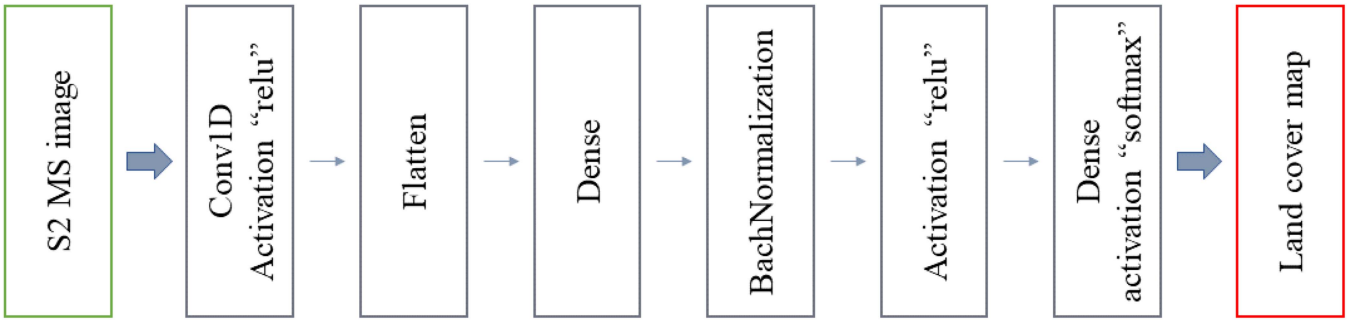

Fig. 3. Architecture of the considered CNN.

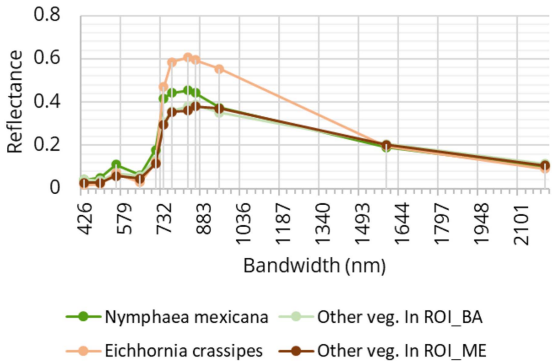

Fig. 4. Spectral signatures of the vegetation differentiated in the training sets, i.e., *Eichhornia crassipes*, other vegetation in ROI_ME, *Nymphaea mexicana*, and other vegetation in ROI_BA.

them). In Fig. 4, the spectral signatures of *Eichhornia crassipes*, *Nymphaea mexicana*, and other vegetation species in ROI_ME and ROI_BA are shown. As it can be seen, the signatures exhibit a similar spectral pattern, but there are some spectral differences between them. These nuances are usually enough for classification algorithms to distinguish them. The fact that invasive plant species can be distinguished from other vegetation species has also been taken into account in other studies [66]. Fig. 4 suggests that the spectral signatures of invasive plant species can be separated from those of other kinds of vegetation species.

F. Image Preprocessing: Dealing With NoData Values

In many research works in which RS techniques have been applied for classification purposes, the analyzed images have a square or rectangular shape. That is because such techniques are often applied to identify every class and all of them are of equal importance in the study. In addition, working with images that are not square or rectangular implies the presence of NoData values, resulting in added difficulty in both preprocessing and data processing. NoData values are values where there is no information about the scene, due mainly to its geometry and not to sensor data capture errors that may result in missing values. Therefore, working with NoData values can be a tedious process, since they have to be considered at GIS level, when data are displayed, and also at coding level, when reading, processing, and writing (saving) the images.

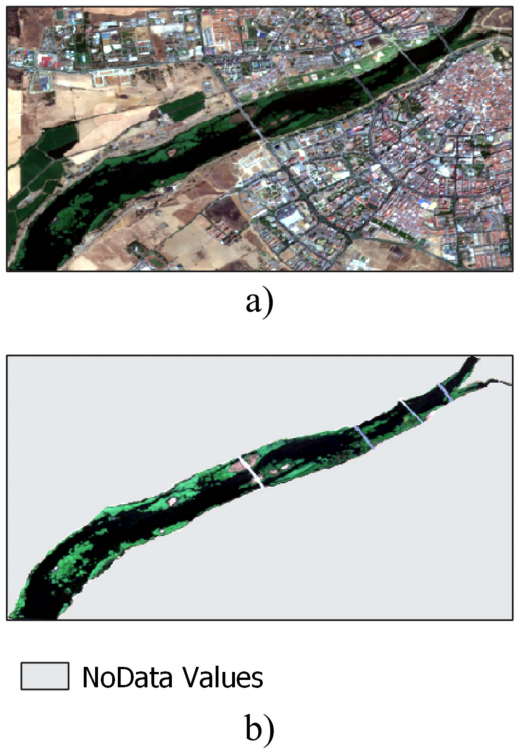

Fig. 5. (a) Full Sentinel-2 image for ROI_BA. (b) Clipped ROI_BA and NoData values present in the image due to its geometry.

In this research, PNOA and Sentinel-2 datasets have been obtained from the mentioned platforms in 8-bit format, and hence pixel values range from 0 to 255 in each spectral band. First, a normalization of these values has been carried out (dividing these values by 255) so that they are displayed in a range from 0 to 1. In order to apply classification techniques only over the areas in which we want to detect aquatic weeds, a previously elaborated mask has been applied to show only the data within each ROI (as shown in Fig. 5). Consequently, datasets have information and NoData values. To deal with NoData values and exclude them from training, prediction, and classification, other values different than the values inside the ROIs have been assigned. The histogram of each dataset has been calculated, and given that the pixels that do contain ROI information saturate the range (0 or 1 values), the dataset format has been changed to 32-bit floating point. Then, NoData values are assigned to

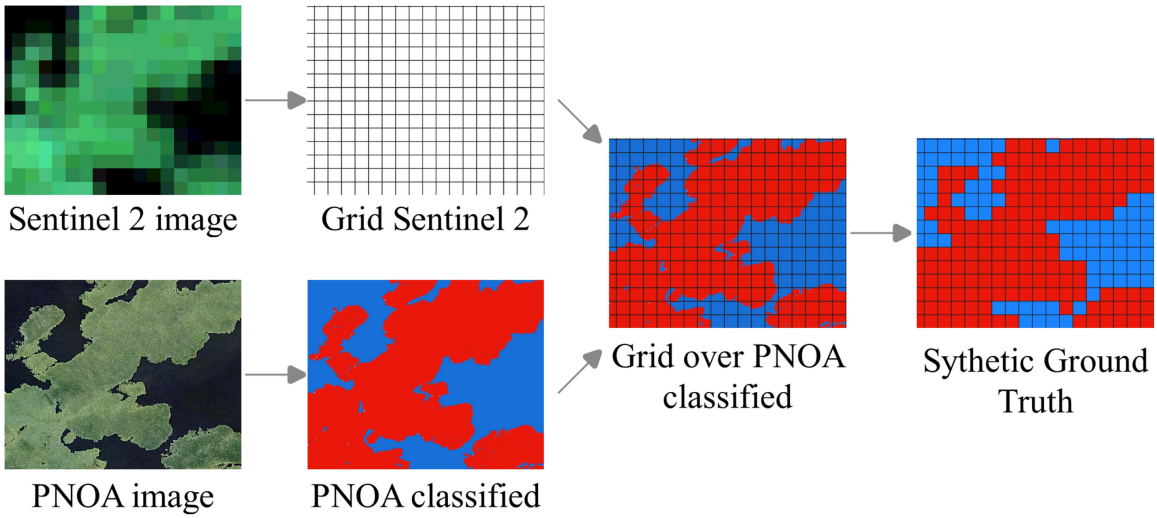

Fig. 6. Main steps in synthetic GT generation.

10 000, avoiding difficulties to handle the data. In addition, at coding level, the ROI mask has been applied so that we only take into account the pixels that are outside the mask to apply the classification techniques.

G. Evaluation of Classification Techniques

In this work, a strategy has been developed to evaluate invasive plants classification. It involves GIS techniques and their implementation in programming languages. Since PNOA MS images have very high spatial resolution, training and validation samples could be chosen by photointerpretation. Furthermore, they can also be used to validate the classification made in the Sentinel-2 dataset. For this purpose, we need to compare the classified pixels in the Sentinel-2 image with the classified pixels in the PNOA dataset. The classification of the latter has been possible by resorting to spatial partitioning. Both datasets have different spatial resolutions; so in order to conduct this operation, we elaborated a synthetic image of the classified PNOA dataset. Thus, the resulting PNOA classified image pixels have 10 m of spatial resolution (the same as Sentinel-2 datasets). In this way, a synthetic GT can be generated and used to compute different evaluation metrics.

1) Window Partitioning for the PNOA Dataset: Since PNOA datasets are very high-resolution images and due to the big dimensions of the ROIs studied, a lot of information is collected. Consequently, the MS data cube requires a large amount of RAM to be able to process the pixels. To solve this problem, we apply the window partitioning methodology presented in [35]. Resulting from this, the PNOA data cube is split in contiguous processing blocks. These neighboring blocks in the spatial domain contain subsets of pixels of the complete dataset with their associated spectral information and can be processed in block by block fashion.

2) Synthetic GT Generation: The main steps in the synthetic GT generation are shown in Fig. 6. First, we consider the Sentinel-2 image with a set of pixels represented by $X_S = x_{S1}, x_{S2}, x_{S3}, \ldots, x_{Sm}$. Then, a vector grid is generated where each cell x_{Gi} is a square of 10 $\times$ 10 m, simulating the contours of the pixel x_{Si}. As a result, the $H \times$W grid (where H is the height and W is the width of the image) has the same dimensions as the Sentinel-2 image, with the same geolocation. On the other hand, the PNOA dataset has been classified by using the RF algorithm, and it is composed of pixels $X_P = \{x_{P1}, x_{P2}, x_{P3}, \ldots, x_{Pm}\}$. Each pixel is labeled as y_{pi}, according to the class where it belongs. The pixels x_{Pi} have a higher spatial resolution than that of x_{Si}. Then, the centroids c_{Pi} of each pixel x_{Pi} are identified, adopting their labels y_{pi} and generating a vector file. Afterwards, a synthetic GT is generated by placing the vector grid on a vector file. Next, each cell x_{ci} of the grid is assigned an attribute table equipped with as many features as labels y_{pi} are present on the vector file. Finally, each cell is assigned with a label y_{pi} by majority voting. Consequently, a synthetic GT is developed resulting in an $H \times$W image with the same number of pixels and spatial resolution as the Sentinel-2 dataset. We emphasize that after having the synthetic GT generated, it was validated and refined by visual comparisons with field observations to guarantee the accuracy of the labels. For illustrative purposes, some synthetic GT scenes generated for the considered ROIs are shown in Fig. 7.

VI. Experimental Results

The results of the application of the considered ML/DL algorithms to the Sentinel-2 datasets are explained in this section. The classification maps and statistics obtained after applying the precision metrics described in the following section are discussed for the Badajoz and Mérida cases. This section concludes with a brief discussion on the obtained results.

A. Metrics for Accuracy Assessment

In order to evaluate the efficiency of different techniques, we assume that the difference between the results and the GT data are due to classification errors. For this purpose, a confusion

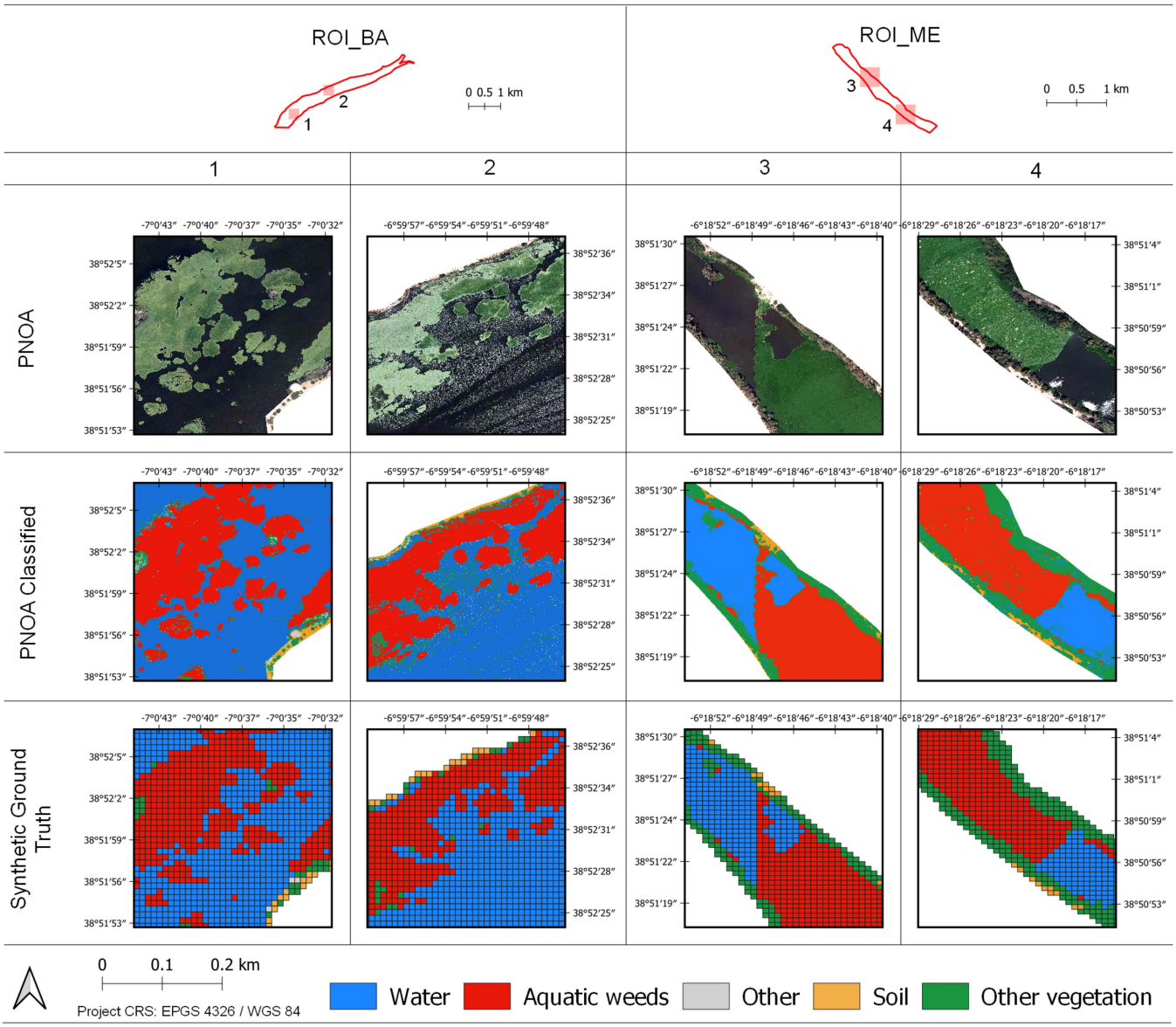

Fig. 7. Some synthetic GT images generated for each considered ROI.

matrix is computed for each of them. In this matrix, true positives (TPs), true negatives (TNs), false positives (FPs), and false negatives (FNs) are shown. The real values are in rows, representing the values in the synthetic GT image. The columns in this matrix contain the predicted values of each classifier. As this study is focused on the detection of aquatic weeds, the confusion matrix is binary (i.e., it indicates whether the invasive plants are detected or not).

The metrics implemented to evaluate the quality of the considered algorithm predictions are overall accuracy [see (3)], user's accuracy [see (4)], producer's accuracy [see (5)] (also known as recall, sensitivity, or TP rate), and F_1 score [see (6)]. Their equations are described as follows:

$$\text{Overall accuracy} = \frac{\text{TP} + \text{TN}}{\text{TP} + \text{TN} + \text{FP} + \text{FN}} \tag{3}$$

$$\text{User's accuracy} = \frac{\text{TP}}{\text{TP} + \text{FP}} \tag{4}$$

$$\text{Producer's accuracy} = \frac{\text{TP}}{\text{TP} + \text{FN}} \tag{5}$$

$$\text{F}_1 \text{ score} = \frac{2 * \text{TP}}{2 * \text{TP} + \text{FP} + \text{FN}}. \tag{6}$$

B. Visual Interpretation of Results: Badajoz Case

Fig. 8 shows the performance of the classification algorithms employed in this study for the detection of aquatic weeds in the Guadiana river (three scenes, one per column, all in Badajoz). In this figure, the first row depicts the PNOA data. The second row depicts the Sentinel-2 data. The third row shows the synthetic GT. The fourth row provides the K-means classification results. The fifth row reports the RF classification results. Finally, the

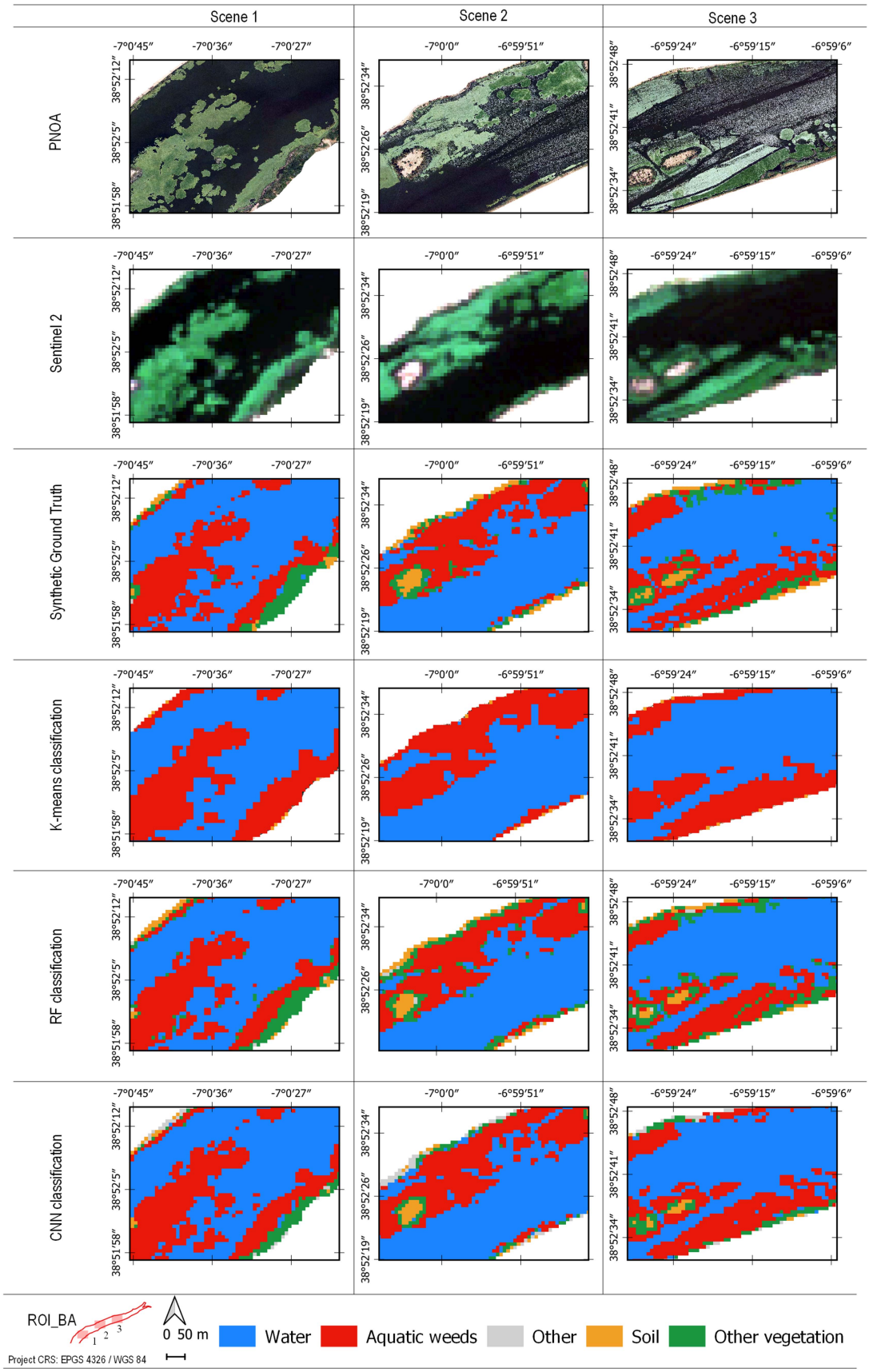

Fig. 8. Classification maps for three representative scenes in ROI_BA (Badajoz).

sixth row contains the CNN classification results. We report results for three representative scenes in ROI_BA. As it is shown, by comparing the RGB image (the PNOA dataset) and the synthetic GT with the results of applying the different classification algorithms on the MS dataset (Sentinel-2 image), we can conclude that they can all detect the presence of aquatic weeds. In the following, we describe the specific results obtained by each algorithm and shown in Fig. 8.

1) Results of K-Means: K-means is an unsupervised algorithm. It has been tested with different numbers of clusters. Five clusters were finally chosen, which are in agreement with the number of classes with which the two supervised algorithms (i.e., RF and CNN) have been trained. In this case, a single cluster is not associated with the aquatic weeds class. Specifically, two clusters represent almost all the aquatic weeds present in the water. However, these clusters do not distinguish the weeds from other types of vegetation. Water can be distinguished well, and part of the soil is also well-differentiated. Another cluster represents different classes, water, and contours of aquatic weeds (mixed pixels). In most cases, this cluster represents areas close to the contours of the masses of aquatic weeds, which are often water areas, although (rarely) they can also contain some pixels associated to aquatic weeds.

2) Results of RF: The RF classification maps have been obtained after a training process with five classes. In the resulting images, aquatic weeds can be distinguished from other classes present in the scenes. Soil, water, and other vegetation areas can be also distinguished. However, some parts of the contour of the masses of aquatic weeds are classified as other vegetation.

3) Results of CNN: The maps obtained by the CNN are in close agreement with the GT. It can be visually seen that this classifier improves the aquatic weeds detection results obtained by the other algorithms.

To conclude this section, Fig. 9 shows the full classification maps obtained by the three considered classifiers for the entire Badajoz scene. It can be seen that supervised classifiers (i.e., RF and CNN) provide more consistent results than the K-means with a better delineation of the river area and the bridges over the river (belonging to the soil class).

C. Visual Interpretation of Results: Mérida case

Fig. 10 shows the obtained classification results in Mérida (three scenes, one per column, all in Mérida). In the following, we describe the results obtained by each classifier in this case.

1) Results of K-Means: After different iterations with different numbers of centroids, we finally considered that the K-means performance with five clusters is the best. With this number of clusters, the classifications of two clusters needed to be grouped to reflect the distribution of invasive plants. Moreover, there are two clusters showing water, which have been grouped with the same color for visualization purposes. Regarding the classification with four clusters, invasive plants were detected, but we could not differentiate them from the vegetation on the river banks.

2) Results of RF: The performance results of the RF classifier improved with regards to the K-means algorithm, as it was already seen in the ROI_BA case study.

3) Results of CNN: The performance results of the CNN classifier improved with regards to the K-means and RF algorithms, as it was already seen in the ROI_BA case study. Specifically, the CNN produced a very good delineation of water bodies and accurate detection results of aquatic invasive plants.

To conclude this section, Fig. 11 shows the full classification maps obtained by the three considered classifiers for the entire Mérida scene. Once again, supervised classifiers (i.e., RF and CNN) provide more consistent results than the K-means with a better identification of soil areas.

D. Statistical Analysis of the Classification Results

The obtained confusion matrices are shown in Fig. 12. It can be seen in these matrices that the accuracy of aquatic weeds detection increases according to the complexity of the algorithm applied. The lowest accuracy is obtained by the K-means algorithm. RF and CNN algorithms outperform K-means and result in similar accuracies, with acceptable FN and FP rates. It is worth noting that the three considered classifiers achieve better performance in ROI_ME than in ROI_BA. As it can be seen in Fig. 9, ROI_BA contains more separate and irregularly shaped masses of aquatic weeds. This leads to the existence of mixed pixels (aquatic weeds with water and aquatic weeds with other vegetation), decreasing the overall classification accuracies. Nevertheless, as it can be seen in Table III (which reports the quantitative metrics calculated, such as the F_1 score, overall accuracy, producer's accuracy, and user's accuracy), the obtained results are close to 1, indicating that good accuracies could be obtained in the ROI_BA case when RF and CNN classifiers are adopted. Table III also gives that the scores for ROI_ME are even superior, with both RF and CNN providing close to optimal results in this case study.

We also compared how accuracies change depending on the number of samples used for the training process. Table IV gives the accuracies for different numbers of training samples. We selected the samples randomly and ran the algorithm ten times, and then we calculated the mean accuracy between executions. Fig. 13 shows that there is not a significant impact in the overall accuracy when reducing the number of samples. This is because a lot of time was spent in this study to carefully select the most representative samples through validation supported by the high-resolution image.

E. Discussion

The two scenarios considered in experiments cover large irregular areas of the Guadiana river (from one margin of the river to the other). Our methodology has been shown to be able to provide accurate classification of invasive plants in large areas of the river, enabling for a detailed monitoring of all river sections affected. Specifically, a preprocessing strategy has been adopted to treat the NoData values present in the pixels outside the analyzed river contour of the whole rectangular image, as the datasets do not have a perfectly rectangular shape.

In addition, different ML/DL classification techniques have been evaluated from clustering algorithms, such as K-means, to more complex supervised classification algorithms, such as RF and CNN. The spatiotemporal distribution of aquatic invasive

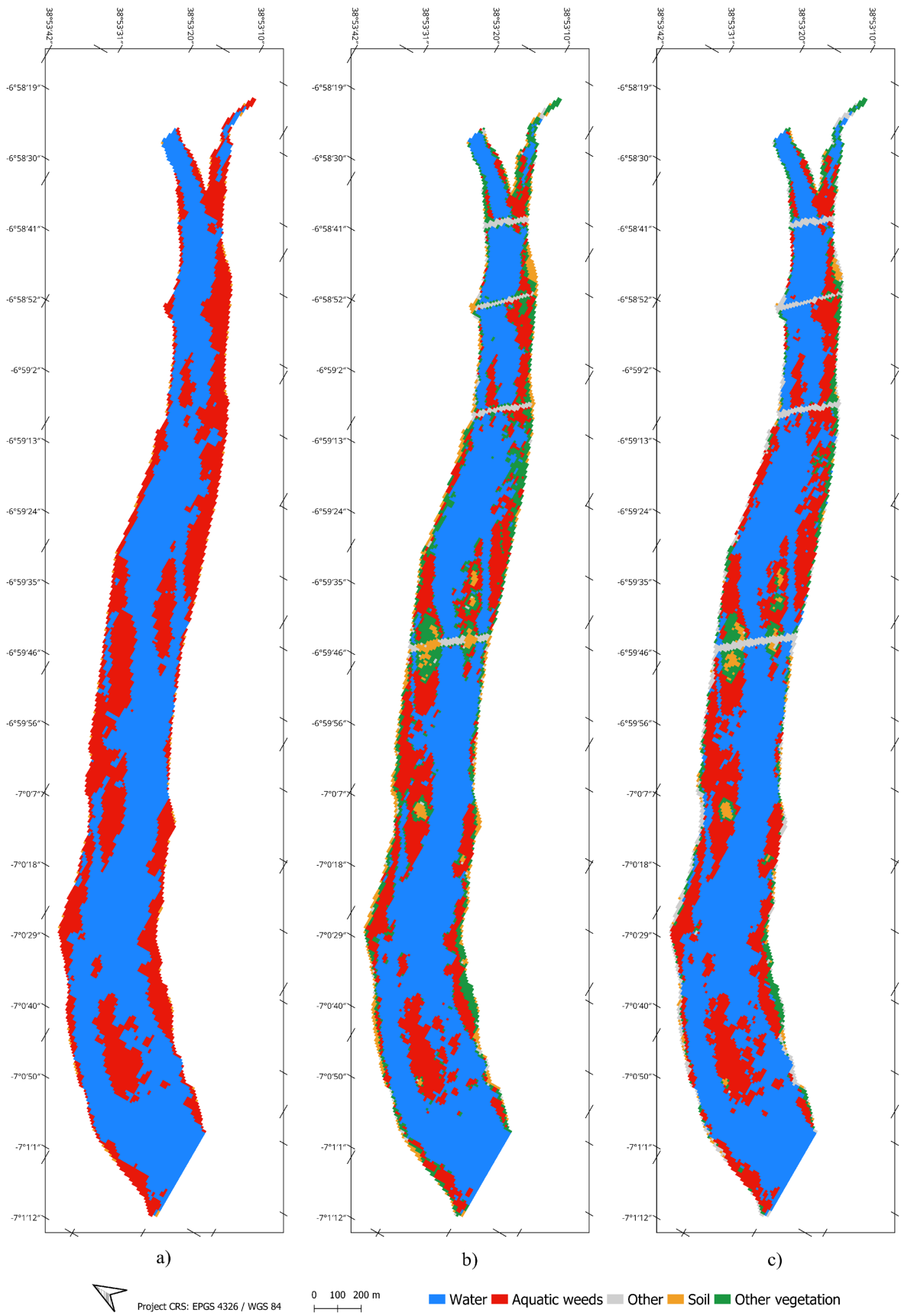

Fig. 9. Classification maps in ROI_BA with different classifiers. (a) K-means. (b) RF. (c) CNN.

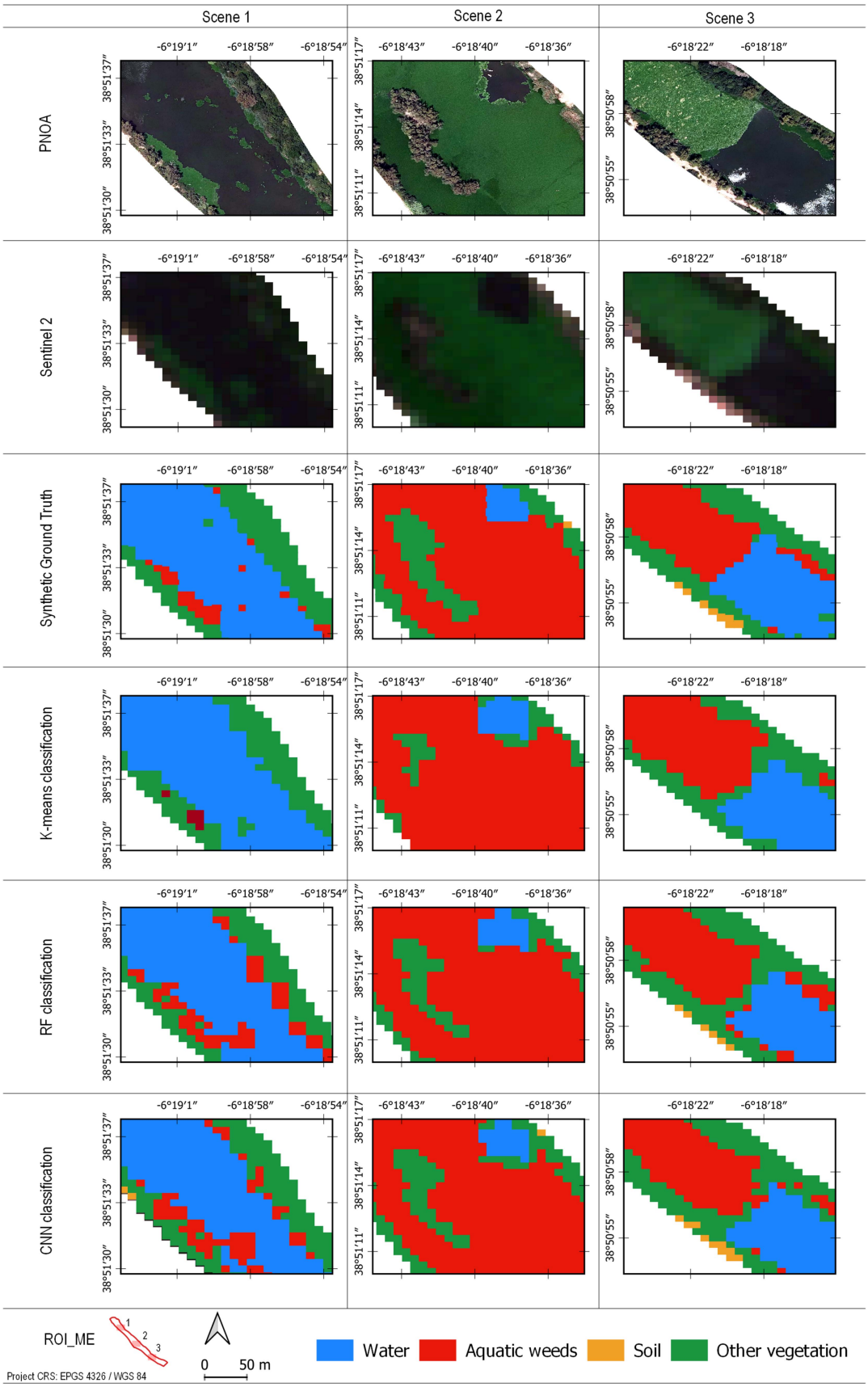

Fig. 10. Classification maps for three representative scenes in ROI_ME (Mérida).

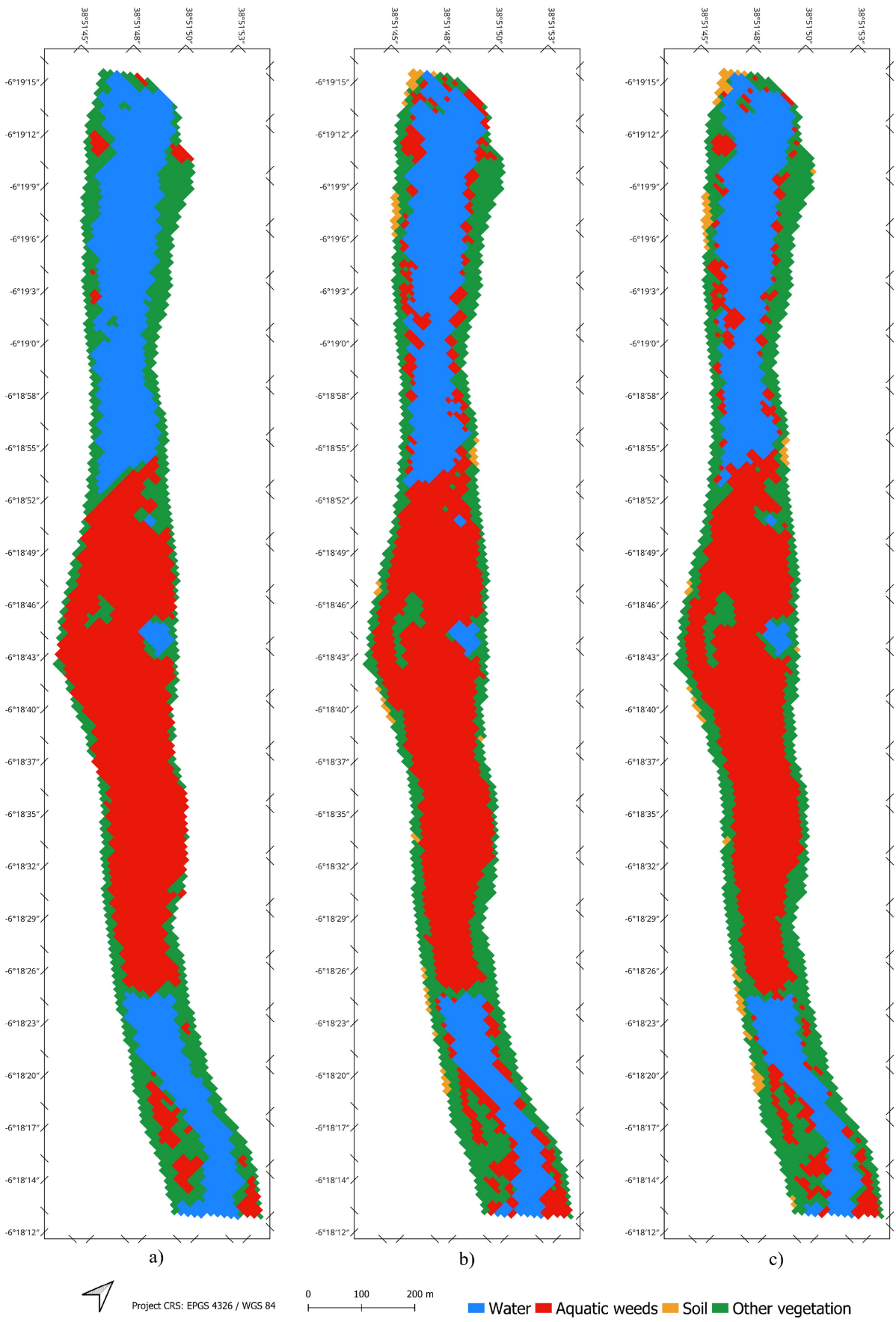

Fig. 11. Classification maps in ROI_ME with different classifiers. (a) K-means. (b) RF. (c) CNN.

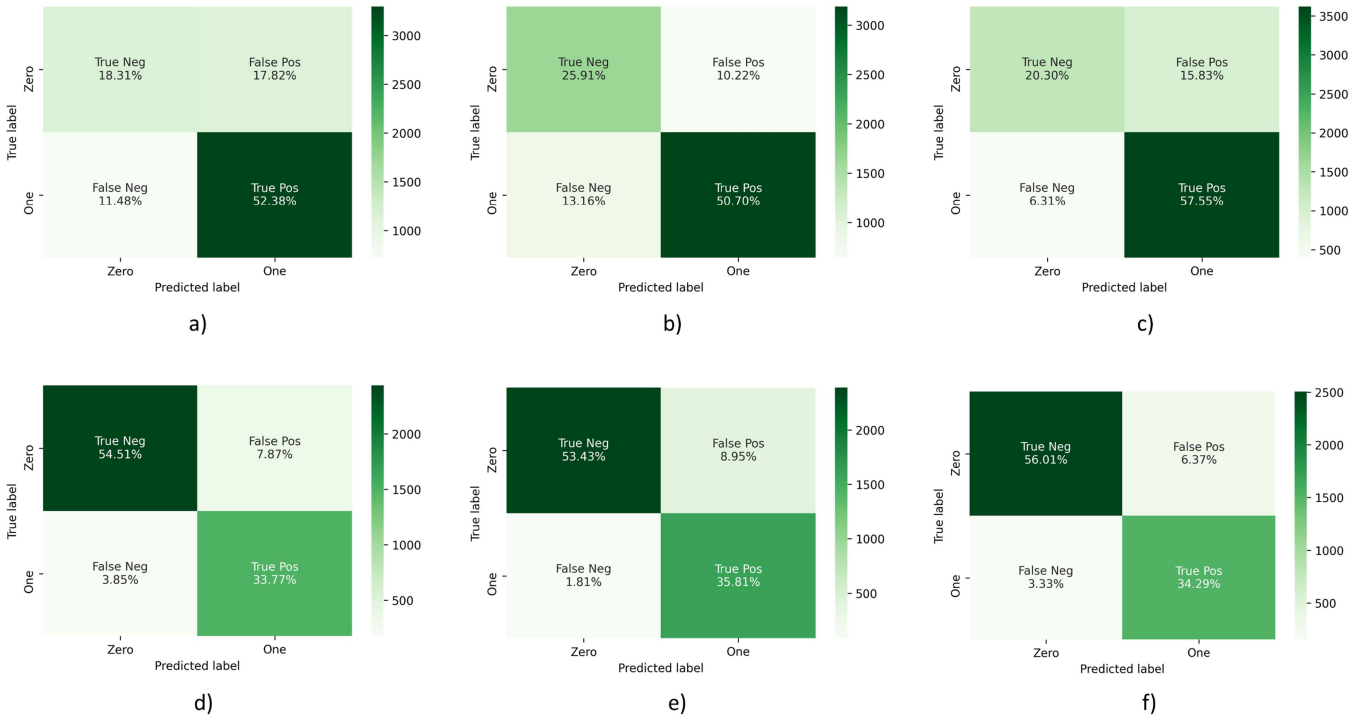

Fig. 12. Confusion matrices. (a) K-means applied to ROI_BA. (b) RF applied to ROI_BA. (c) CNN applied to ROI_BA. (d) K-means applied to ROI_ME. (e) RF applied to ROI_ME. (f) CNN applied to ROI_ME.

TABLE III
PERFORMANCE METRICS FOR THE BADAJOZ AND MÉRIDA CASES

		Overall accuracy	User's accuracy	Producer's accuracy	F_1 score
Badajoz case	K-means	0.707	0.746	0.820	0.781
	RF	0.766	0.832	0.794	0.813
	CNN	0.779	0.784	0.901	0.839
Mérida case	K-means	0.883	0.881	0.898	0.852
	RF	0.892	0.800	0.952	0.869
	CNN	0.903	0.843	0.911	0.876

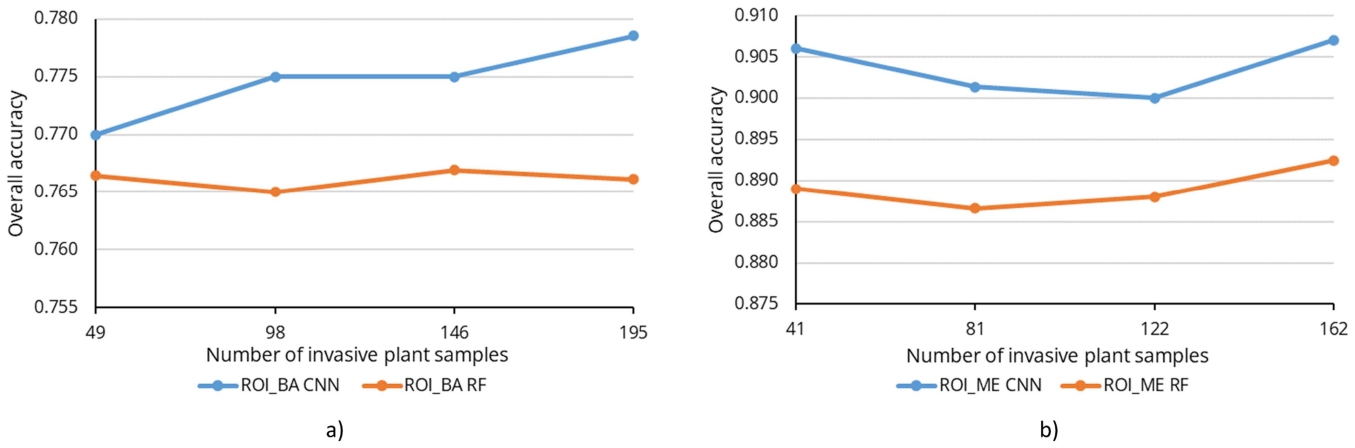

Fig. 13. Graphical representation of the overall classification accuracy obtained using different numbers of training samples. (a) ROI_BA. (b) ROI_ME.

TABLE IV
OVERALL CLASSIFICATION ACCURACY OBTAINED USING DIFFERENT NUMBERS OF TRAINING SAMPLES FOR THE BADAJOZ AND MÉRIDA CASES

Badajoz case	Number of samples	**41**	**81**	**122**	**162**
	RF	0.766	0.765	0.767	0.766
	CNN	0.770	0.775	0.775	0.779
Mérida case	Number of samples	**49**	**98**	**146**	**195**
	RF	0.889	0.887	0.888	0.892
	CNN	0.900	0.902	0.900	0.903

The bold entities indicate the best result of the comparison methods.

plants has been accurately mapped by RF and CNN classifiers using a limited number of training samples. Our results demonstrate the success of these approaches in terms of quantitative accuracy and visual appearance of the obtained results.

Specifically, we have observed that CNNs provide better classification results and can therefore detect aquatic invasive plants very accurately. They are followed in decreasing order of accuracy by RF and K-means. The advantage of using K-means is the fact that the algorithm is unsupervised, and hence does not require collecting training samples. On the other hand, K-means needs to identify the classes detected by the clusters, which may be difficult in practice.

Another important observation is that better results are obtained when the masses are distributed in the water surface, forming fewer blankets than in the case in which they are distributed in separated masses and with irregular contours, which favors the existence of mixed pixels that decrease the overall accuracy. In this sense, training supervised classifiers, such as RF and CNN, can be useful to carry out predictions in other river datasets. In this study, these classifiers have achieved reasonable accuracies (between 77% and 90% in terms of overall accuracy) with a small percentage of training samples (only 2.58% of the available labeled samples in the Badajoz case and 10.08% of the available labeled samples in the Mérida case). Thus, considering the classifier that has obtained the highest accuracy (CNN), the area occupied by the invasive plants is about 18 ha in ROI_ME and about 46 ha in ROI_BA.

Moreover, the results obtained show that similar classification accuracies can be achieved with high-resolution images, such as PNOA data (which are expensive and costly to process), than with medium-resolution images, such as Sentinel-2 images (which are free and require less processing time). The strategy developed for validation of the results has been possible thanks to the synthetic GT generated from high-resolution classified images that required using a window processing strategy (due to the large amount of RAM memory needed).

To conclude this section, we note that ML/DL algorithms can also be applied to the PNOA dataset, but the classification accuracy cannot be calculated because the PNOA image is the one that we use as our baseline for creating the GT. Sentinel-2 data are easier to work with due to their size (PNOA images are about 800 times heavier due to their high spatial resolution). This is why our goal is to detect invasive plants in Sentinel-2 medium spatial resolution images instead of high resolution expensive PNOA flights that are used in this work as a starting point for generating a high-quality GT.

VII. CONCLUSION

In this study, we have developed a full processing chain for automatic detection of aquatic invasive plants in satellite images. Specifically, our methodology comprises preprocessing, processing, and evaluation stages, able to accurately geolocate invasive vegetation weeds present in the Guadiana river, Spain, achieving high detection accuracies. In our work, supervised classifiers performed better than unsupervised ones, not only because RF and CNN can provide good results with a limited number of training samples, but also because the unsupervised algorithm (K-means) ultimately needs a supervised interpretation process (based on analyzing high-resolution images to combine some of the obtained clusters). The use of one algorithm or another depends on the requirements of each case study, but in our context, the CNN classifier was regarded as the best tool of choice.

Continuous monitoring and control of aquatic invasive plants require early detection of the growth of existing masses in the water. To achieve this goal, future work will be oriented toward the development of methods able to assess the spatiotemporal evolution of aquatic weeds, given that Sentinel-2 captures images with a five-day revisit time, which allows to conduct change detection studies in that time frame. In addition, other DL approaches can be considered in future studies. For instance, the spatial information of the input image may be considered besides the spectral signature of each pixel by using a spatial CNN (CNN2D) classifier. A spatial–spectral CNN (CNN3D) architecture may also be used for even more refined classification.

ACKNOWLEDGMENT

The authors would like to thank *Confederación Hidrográfica del Guadiana* for corroborating the geolocation of invasive plants species in the two scenarios analyzed and Associate Editor and the two Anonymous Reviewers for their outstanding comments and suggestions that greatly helped us to improve the technical content and presentation of our manuscript.

REFERENCES

[1] M. Sánchez, A. Cuartero, M. Barrena, and A. Plaza, "A new method for positional accuracy analysis in georeferenced satellite images without independent ground control points," *Remote Sens.*, vol. 12, 2020, Art. no. 4132.

[2] A. Plaza, J. Plaza, A. Paz, and S. Sánchez, "Parallel hyperspectral image and signal processing [applications corner]," *IEEE Signal Process. Mag.*, vol. 28, no. 3, pp. 119–126, May 2011.

[3] E. C. Enoguanbhor, F. Gollnow, J. O. Nielsen, T. Lakes, and B. B. Walker, "Land cover change in the Abuja city-region, Nigeria: Integrating GIS and remotely sensed data to support land use planning," *Sustainability*, vol. 11, 2019, Art. no. 1313.

[4] J. Cavender-Bares, J. A. Gamon, and P. A. Townsend, *Remote Sensing of Plant Biodiversity*. Berlin, Germany: Springer, 2020.

[5] K. Kaku, "Satellite remote sensing for disaster management support: A holistic and staged approach based on case studies in Sentinel Asia," *Int. J. Disaster Risk Reduction*, vol. 33, pp. 417–432, 2019.

[6] M. Tadese, L. Kumar, R. Koech, and B. K. Kogo, "Mapping of land-use/land-cover changes and its dynamics in Awash River Basin using remote sensing and GIS," *Remote Sens. Appl.: Soc. Environ.*, vol. 19, 2020, Art. no. 100352.

[7] D. Apostolopoulos and K. Nikolakopoulos, "A review and meta-analysis of remote sensing data, GIS methods, materials and indices used for monitoring the coastline evolution over the last twenty years," *Eur. J. Remote Sens.*, vol. 54, pp. 240–265, 2021.

[8] V. H. Smith and D. W. Schindler, "Eutrophication science: Where do we go from here?," *Trends Ecol. Evol.*, vol. 24, pp. 201–207, Apr. 2009.

[9] R. G. Hartzler and D. D. Buhler, *Ecological Management of Agricultural Weeds*. Cambridge, U.K.: Cambridge Univ. Press, 2001.

[10] S. Patel, *Threats, Management and Envisaged Utilizations of Aquatic Weed Eichhornia Crassipes: An Overview*, vol. 11. Berlin, Germany: Springer, Jul. 2012.

[11] A. M. Villamagna and B. R. Murphy, "Ecological and socio-economic impacts of invasive water hyacinth *(Eichhornia crassipes)*: A review," *Freshwater Biol.*, vol. 55, pp. 282–298, 2010.

[12] A. Hussner, "Alien aquatic plant species in European countries," *Weed Res.*, vol. 52, pp. 297–306, 2012.

[13] N. Hanley and M. Roberts, "The economic benefits of invasive species management," *People Nat.*, vol. 1, pp. 124–137, 2019.

[14] K. J. Murphy, "Aquatic weed problems and their management: A review. II. Physical control measures," *Crop Protection*, vol. 7, pp. 283–302, 1988.

[15] K. J. Murphy, "Aquatic weed problems and their management: A review I. The worldwide scale of the aquatic weed problem," *Crop Protection*, vol. 7, pp. 232–248, 1988.

[16] E. O. O. Gangstad, *Weed Control Methods for River Basin Management*. Boca Raton, FL, USA: CRC Press, 2018.

[17] D. Bubenheim, V. Genovese, J. D. Madsen, and E. Hard, "Remote sensing and mapping of floating aquatic vegetation in the Sacramento–San Joaquin River Delta," *J. Aquatic Plant Manage.*, vol. 59, pp. 46–54, 2021.

[18] B. Song and K. Park, "Detection of aquatic plants using multispectral UAV imagery and vegetation index," *Remote Sens.*, vol. 12, 2020, Art. no. 387.

[19] E. K. Cheruiyot, C. Mito, M. Menenti, B. Gorte, R. Koenders, and N. Akdim, "Evaluating MERIS-based aquatic vegetation mapping in Lake Victoria," *Remote Sens.*, vol. 6, pp. 7762–7782, 2014.

[20] M. Schmidt, "Monitoring aquatic weeds in a river system using SPOT 5 satellite imagery," *J. Appl. Remote Sens.*, vol. 4, 2010, Art. no. 043528.

[21] E. L. Hestir et al., "Identification of invasive vegetation using hyperspectral remote sensing in the California Delta ecosystem," *Remote Sens. Environ.*, vol. 112, pp. 4034–4047, 2008.

[22] K. J. Sheffield, D. Clements, D. J. Clune, A. Constantine, and T. M. Dugdale, "Detection of aquatic alligator weed (*Alternanthera philoxeroides*) from aerial imagery using random forest classification," *Remote Sens.*, vol. 14, 2022, Art. no. 2674.

[23] V. Akbari et al., "Monitoring aquatic weeds in indian wetlands using multitemporal remote sensing data with machine learning techniques," in *Proc. IEEE Int. Geosci. Remote Sens. Symp.*, 2021, pp. 6847–6850.

[24] C. Nyamekye et al., "Evaluating the spatial and temporal variations of aquatic weeds (Biomass) on Lower Volta River using multi-sensor Landsat Images and machine learning," *Heliyon*, vol. 7, 2021, Art. no. e07080.

[25] C. M. Viana, I. Girão, and J. Rocha, "Long-term satellite image time-series for land use/land cover change detection using refined open source data in a rural region," *Remote Sens.*, vol. 11, 2019, Art. no. 1104.

[26] A. D. Kulkarni and B. Lowe, "Random forest algorithm for land cover classification," *Int. J. Recent Innov. Trends Comput. Commun.*, vol. 4, pp. 58–63, 2016.

[27] S. E. Jodzani, B. A. Johnson, and D. Chen, "Comparing deep neural networks, ensemble classifiers, and support vector machine algorithms," *Remote Sens.*, vol. 11, 2019, Art. no. 1713.

[28] V. L. Diengdoh, S. Ondei, M. Hunt, and B. W. Brook, "A validated ensemble method for multinomial land-cover classification," *Ecological Inform.*, vol. 56, 2020, Art. no. 101065.

[29] L. Ma, Y. Liu, X. Zhang, Y. Ye, G. Yin, and B. A. Johnson, "Deep learning in remote sensing applications: A meta-analysis and review," *ISPRS J. Photogrammetry Remote Sens.*, vol. 152, pp. 166–177, 2019.

[30] Z.-Q. Zhao, P. Zheng, S.-T. Xu, and X. Wu, "Object detection with deep learning: A review," *IEEE Trans. Neural Netw. Learn. Syst.*, vol. 30, no. 11, pp. 3212–3232, Nov. 2019.

[31] D. Zeng et al., "Deep learning for scene classification: A survey," vol. abs/2101.10531, 2021, *arXiv:2101.1053*. [Online]. Available: https://arxiv.org/abs/2101.10531

[32] M. E. Paoletti, J. M. Haut, J. Plaza, and A. Plaza, "A new deep convolutional neural network for fast hyperspectral image classification," *ISPRS J. Photogrammetry Remote Sens.*, vol. 145, pp. 120–147, 2018.

[33] D. He, Y. Zhong, X. Wang, and L. Zhang, "Deep convolutional neural network framework for subpixel mapping," *IEEE Trans. Geosci. Remote Sens.*, vol. 59, no. 11, pp. 9518–9539, Nov. 2021.

[34] L. Pádua et al., "Water hyacinth (*Eichhornia crassipes*) detection using coarse and high resolution multispectral data," *Drones*, vol. 6, 2022, Art. no. 47.

[35] E. C. Rodríguez-Garlito and A. Paz-Gallardo, "Efficiently mapping large areas of olive trees using drones in Extremadura, Spain," *IEEE J. Miniaturization Air Space Syst.*, vol. 2, no. 3, pp. 148–156, Sep. 2021.

[36] K. H. Thamaga and T. Dube, "Remote sensing of invasive water hyacinth (*Eichhornia crassipes*): A review on applications and challenges," *Remote Sens. Appl.: Soc. Environ.*, vol. 10, pp. 36–46, 2018.

[37] Accessed: Jun. 2022. [Online]. Available: https://www.chguadiana.es/

[38] J. A. Coetzee, M. P. Hill, T. Ruiz-Téllez, U. Starfinger, and S. Brunel, "Monographs on invasive plants in Europe n° 2: *Eichhornia crassipes* (Mart.) Solms," *Botany Lett.*, vol. 164, pp. 303–326, 2017.

[39] A. Rodríguez-Merino, P. García-Murillo, S. Cirujano, and R. Fernández-Zamudio, "Predicting the risk of aquatic plant invasions in Europe: How climatic factors and anthropogenic activity influence potential species distributions," *J. Nat. Conservation*, vol. 45, pp. 58–71, 2018.

[40] F. C. F. Aguiar and M. T. Ferreira, "Plant invasions in the rivers of the Iberian Peninsula, South-Western Europe: A review," *Plant Biosyst.*, vol. 147, pp. 1107–1119, 2013.

[41] Accessed: Jun. 2022. [Online]. Available: http://www.invasep.eu/

[42] Accessed: Jun. 2022. [Online]. Available: https://camaloteaceca.eu/?page_id=620&lang=en

[43] C. H. del Guadiana, "Gobernanza y estrategias para la lucha contra las especies exóticas invasoras en la cuenca del guadiana," 2021. Accessed: Jun. 2021. [Online]. Available: https://www.chguadiana.es/sites/default/files/2021-05/REVISI%C3%93N_ESTRATEGIA%20DE%20EEI%202021%20COMPLETA_firmada.pdf

[44] L. Alonso, J. Picos, G. Bastos, and J. Armesto, "Detection of very small tree plantations and tree-level characterization using open-access remote-sensing databases," *Remote Sens.*, vol. 12, 2020, Art. no. 2276.

[45] M. Padial-Iglesias, P. Serra, M. Ninyerola, and X. Pons, "A framework of filtering rules over ground truth samples to achieve higher accuracy in land cover maps," *Remote Sens.*, vol. 13, 2021, Art. no. 2662.

[46] F. Alonso-Sarria, C. Valdivieso-Ros, and F. Gomariz-Castillo, "Isolation forests to evaluate class separability and the representativeness of training and validation areas in land cover classification," *Remote Sens.*, vol. 11, 2019, Art. no. 3000.

[47] Accessed: Jun. 2022. [Online]. Available: https://inspire.ec.europa.eu/

[48] Accessed: Jun. 2022. [Online]. Available: https://pnoa.ign.es/

[49] E. Kroupi et al., "Deep convolutional neural networks for land-cover classification with Sentinel-2 images," *J. Appl. Remote Sens.*, vol. 13, Jun. 2019, Art. no. 024525, doi: 10.1117/1.JRS.13.024525.

[50] D. Phiri et al., "Sentinel-2 data for land cover/use mapping: A review," *Remote Sens.*, vol. 12, 2020, Art. no. 2291.

[51] Accessed: Jun. 2022. [Online]. Available: https://sentinel.esa.int/web/sentinel/missions/sentinel-2

[52] Copernicus-sentinel-2. Accessed: Jun. 2022. [Online]. Available: https://eoportal.org/web/eoportal/satellite-missions/c-missions/copernicus-sentinel-2

[53] J. E. Ball, D. T. Anderson, and C. S. Chan, "A comprehensive survey of deep learning in remote sensing: Theories, tools and challenges for the community," *J. Appl. Remote Sens.*, vol. 11, 2017, Art. no. 042609.

[54] L. Goodfellow and A. Courville, *Deep Learning*. Cambridge, MA, USA: MIT Press, 2016.

[55] Y. Bengio, *Learning Deep Architectures for AI*, vol. 2. Boston, MA, USA: Now Publishers, 2009.

[56] M. E. Paoletti, J. M. Haut, J. Plaza, and A. Plaza, "Deep learning classifiers for hyperspectral imaging: A review," *ISPRS J. Photogrammetry Remote Sens.*, vol. 158, pp. 279–317, 2019.

[57] L. Breiman, "Random forests," *Mach. Learn.*, vol. 45, pp. 5–32, 2001.

[58] R. E. Blahut, *Fast Algorithms for Signal Processing*. New York, NY, USA: Cambridge Univ. Press, 2010.

[59] T. Hastie, J. Friedman, and R. Tibshirani, *The Elements of Statistical Learning*. New York, NY, USA: Springer, 2009.

[60] Y. Lecun, Y. Bengio, and G. Hinton, "Deep learning," *Nature*, vol. 521, pp. 436–444, 2015.

[61] L. Zhang, L. Zhang, and B. Du, "Deep learning for remote sensing data: A technical tutorial on the state of the art," *IEEE Geosci. Remote Sens. Mag.*, vol. 4, no. 2, pp. 22–40, Jun. 2016.
[62] W. Hu, Y. Huang, L. Wei, F. Zhang, and H. Li, "Deep convolutional neural networks for hyperspectral image classification," *J. Sensors*, vol. 2015, 2015, Art. no. 258619.
[63] Accessed: Jun. 2022. [Online]. Available: https://centrodedescargas.cnig.es/CentroDescargas/
[64] Accessed: Jun. 2022. [Online]. Available: https://www.sentinel-hub.com/explore/sentinelplayground/
[65] S. Madry, *Introduction to QGIS: Open Source Geographic Information System*. Locate Press, 2021. [Online]. Available: https://books.google.es/books?id=biJozgEACAAJ
[66] K. H. Thamaga and T. Dube, "Understanding seasonal dynamics of invasive water hyacinth (*Eichhornia crassipes*) in the Greater Letaba river system using Sentinel-2 satellite data," *GIScience Remote Sens.*, vol. 56, pp. 1355–1377, 2019.

Elena C. Rodríguez-Garlito (Student Member, IEEE) received the B.Sc. degree in civil engineering and the M.Sc. degree in geographical information systems and remote sensing, in 2013 and 2014, respectively, from the University of Extremadura, Cáceres, Spain, where she is currently working toward the Ph.D. degree in the area of invasive aquatic plants detection using remote sensing techniques, with predoctoral contracts for the training of Doctors in public RD centers belonging to the Extremadura System of Science, Technology, and Innovation.

She is currently a Member of Hyperspectral Computing Laboratory, Department of Technology of Computers and Communications, University of Extremadura. Her research interests include GIS, remote sensing, and machine/deep learning.

Abel Paz-Gallardo received the B.S. degree in computer engineering and the M.Sc. and Ph.D. degrees in computer science from the University of Extremadura, Cáceres, Spain, in 2007, 2009, and 2011, respectively.

During 2006 and 2007, he was a Research Assistant with Computer Architecture Department, University of Extremadura, where he became an Associate Professor in 2008. At the same time, he started working with Minimally Invasive Surgery Center Jesús Usón, Cáceres. In 2010, he started working with Bull Spain S.A. to deploy at CETA-Ciemat, Trujillo, Spain, the biggest GPGPU Cluster in Spain and one of the biggest ones in Europe. Since November 2010, he has been an Associate Professor with Computer Architecture Department. From October 2011 to July 2018, he was the IT Manager (CIO) with CETA-Ciemat, where he achieved the GPU Research Centre mention from NVIDIA as Principal Investigator. Since July 2018, he has been the Chief Information Officer with Greenfield Technologies, a precision agriculture company that provides recommendations to farmers through the use of different innovative technologies, such as drones, satellites, sensors, and artificial intelligence, and applied research. He has participated in more than 40 international projects and has authored or coauthored more than 40 publications, including 14 journal citation report papers (most of them published by IEEE journals) and more than 30 peer-reviewed international conference papers. His research interests include remotely sensed hyperspectral image analysis, signal processing, and efficient implementations of large-scale scientific problems on high-performance computing architectures, such as clusters and graphical processing units.

Dr. Paz-Gallardo was the recipient of the IEEE Signal Processing Magazine Best Column Award Paper from the IEEE Signal Processing Society in November 2015.

Antonio Plaza (Fellow, IEEE) received the M.Sc. and Ph.D. degrees in computer engineering from the University of Extremadura, Cáceres, Spain, in 1999 and 2002, respectively.

He is currently a Full Professor and the Head of Hyperspectral Computing Laboratory, Department of Technology of Computers and Communications, University of Extremadura. He has authored or coauthored more than 600 publications, including 364 JCR journal papers (265 in IEEE journals), 24 book chapters, and 330 peer-reviewed conference proceeding papers, in the field of his research interests, including hyperspectral data processing and parallel computing of remote sensing data.

Prof. Plaza has guest edited ten special issues on hyperspectral remote sensing for different journals. He is a Fellow of IEEE "for contributions to hyperspectral data processing and parallel computing of Earth observation data" and a Member of Academia Europaea, The Academy of Europe. He was the recipient of the Recognition of Best Reviewers of IEEE GEOSCIENCE AND REMOTE SENSING LETTERS (in 2009), the Recognition of Best Reviewers of IEEE TRANSACTIONS ON GEOSCIENCE AND REMOTE SENSING (in 2010) for which he was an Associate Editor in 2007–2012, the Best Column Award of the IEEE Signal Processing Magazine in 2015, the 2013 Best Paper Award of the IEEE JOURNAL OF SELECTED TOPICS IN APPLIED EARTH OBSERVATIONS AND REMOTE SENSING (JSTARS), the most highly cited paper (2005–2010) in the Journal of Parallel and Distributed Computing, and best paper awards at the IEEE Workshop on Hyperspectral Image and Signal Processing: Evolution in Remote Sensing, the IEEE International Conference on Space Technology, and the IEEE Symposium on Signal Processing and Information Technology. He is an Associate Editor for IEEE ACCESS (receiving the recognition of Outstanding Associate Editor for the journal in 2017) and was a Member of the Editorial Board of *IEEE Geoscience and Remote Sensing Newsletter* (2011–2012), *IEEE Geoscience and Remote Sensing Magazine* (2013), and of the steering committee of the JSTARS. He was the Director of Education Activities for the IEEE Geoscience and Remote Sensing Society (GRSS) in 2011 and 2012, and the President of the Spanish Chapter of IEEE GRSS in 2012 and 2016. He is a Chair of the Publications Awards Committee of IEEE GRSS and a Vice Chair of the Fellow Evaluations Committee of IEEE GRSS. He has reviewed more than 500 manuscripts for more than 50 different journals. He was the Editor-in-Chief of IEEE TRANSACTIONS ON GEOSCIENCE AND REMOTE SENSING journal for five years (2013–2017) and IEEE JOURNAL ON MINIATURIZATION FOR AIR AND SPACE SYSTEMS (2019–2020). He has been included in the 2018–2021 Highly Cited Researchers List (Clarivate Analytics).